Song *et al.* *Soft Sci* 2022;2:13
DOI: 10.20517/ss.2022.11

Soft Science

Research Article

Open Access

Reliable metal alloy contact for $Mg_{3+\delta}Bi_{1.5}Sb_{0.5}$ thermoelectric devices

Shaowei Song[1], Zhongxin Liang[2], Congcong Xu[1], Yu Wang[1,2], Xin Shi[1], Wuyang Ren[1,3], Zhifeng Ren[1,*]

[1]Department of Physics and Texas Center for Superconductivity at University of Houston (TcSUH), University of Houston, Houston, TX 77204, USA.
[2]Materials Science and Engineering Program, University of Houston, Houston, TX 77204, USA.
[3]Institute of Fundamental and Frontier Sciences, University of Electronic Science and Technology of China, Chengdu 610054, Sichuan, China.

[*]**Correspondence to:** Prof. Zhifeng Ren, Department of Physics and Texas Center for Superconductivity at University of Houston (TcSUH), University of Houston, Houston, TX 77204, USA. E-mail: zren@uh.edu

How to cite this article: Song S, Liang Z, Xu C, Wang Y, Shi X, Ren W, Ren Z. Reliable metal alloy contact for Mg_{3+} $Bi_{1.5}Sb_{0.5}$ thermoelectric devices. *Soft Sci* 2022;2:13. https://dx.doi.org/10.20517/ss.2022.11

Received: 31 May 2022 **First Decision:** 7 Jul 2022 **Revised:** 14 Jul 2022 **Accepted:** 19 Jul 2022 **Available online:** 2 Aug 2022

Academic Editor: Cunjiang Yu **Copy Editor:** Fangling Lan **Production Editor:** Fangling Lan

Abstract

Proper contacts between thermoelectric (TE) materials and electrodes are critical for TE power generation or refrigeration. The Bi-rich n-type Zintl material $Mg_{3+\delta}Bi_{2-x}Sb_x$ exhibits very good TE performance near room temperature, which makes $Mg_{3+\delta}Bi_{2-x}Sb_x$-based compounds highly promising candidates to replace the $Bi_2Te_{3-y}Se_y$ alloys, but ideal contacts that can match their TE performance have not yet been well studied. Here we investigate different metal (Ni and Fe) and metal alloy (NiFe, NiCr, NiCrFe, and stainless steel) contacts on n-type $Mg_{3+\delta}Bi_{1.5}Sb_{0.5}$. It is first shown that the low Schottky barrier and narrow depletion region resulting from the band degeneracy and high carrier concentration of a heavily doped TE material are beneficial for the formation of a low-resistivity ohmic contact with a metal or a metal alloy. Most fully optimized TE materials can take advantage of this. Second, it is found that the NiFe/$Mg_{3+\delta}Bi_{1.5}Sb_{0.5}$ contact exhibits excellent thermal stability and the lowest ohmic contact resistivity among those studied after aging for over 2100 h, which is attributed to the formation of metallic NiMgBi between the NiFe and $Mg_{3+\delta}Bi_{1.5}Sb_{0.5}$ layers. As a buffer phase, NiMgBi can effectively prevent elemental diffusion without negatively affecting the electron transport. Benefiting from such low contact resistance, a $Mg_{3+\delta}Bi_{1.5}Sb_{0.5}$/$Bi_{0.4}Sb_{1.6}Te_3$ unicouple exhibits competitive conversion efficiency, 6% with a 150 K temperature difference and a hot-side temperature of 448 K.

© The Author(s) 2022. **Open Access** This article is licensed under a Creative Commons Attribution 4.0 International License (https://creativecommons.org/licenses/by/4.0/), which permits unrestricted use, sharing, adaptation, distribution and reproduction in any medium or format, for any purpose, even commercially, as long as you give appropriate credit to the original author(s) and the source, provide a link to the Creative Commons license, and indicate if changes were made.

Keywords: Thermoelectric power generator, ohmic contact, $Mg_{3+\delta}Bi_{1.5}Sb_{0.5}$, NiFe alloy, energy conversion

INTRODUCTION

$Mg_{3+\delta}Sb_{2-x}Bi_x$ Zintl compounds have attracted considerable attention due to their remarkable thermoelectric (TE) performance at room and intermediate temperatures[1-3]. In particular, the n-type compounds in this system exhibit near-room-temperature performance comparable to that of the commercial n-type $Bi_2Te_{3-y}Se_y$ alloys[4], which have commonly been used for TE refrigeration and power generation in the past few decades. However, n-type $Mg_{3+\delta}Sb_{2-x}Bi_x$ materials have unparalleled advantages over the n-type $Bi_2Te_{3-y}Se_y$ compounds in terms of material costs and mechanical strength, leading to an alternative solution of pairing n-type $Mg_{3+\delta}Sb_{2-x}Bi_x$ materials with p-type Bi_2Te_3-based materials for TE device assembly. Since the stability and mass production of n-type $Mg_{3+\delta}Sb_{2-x}Bi_x$ have been explored recently[5-7], seeking the proper contacts for n-type $Mg_{3+\delta}Sb_{2-x}Bi_x$ is essential to guarantee long service life and high conversion efficiency for the assembled TE devices.

In some cases, although the TE materials used in a device exhibit high performance, contact-related instability becomes its weakest aspect. This can partially explain why the actual conversion efficiency of a TE module is always below its theoretical value, or why the exceptional *zT* values of the TE materials are not reflected in the conversion efficiency of the device[8,9]. Reliable contacts are thus critical for a TE device. Requirements for a good contact include low electrical and thermal contact resistivity, excellent stability, and high thermal-failure resistance. It is desired that the contact layers have proper wettability with the TE legs for firm welding between the TE leg and the electrodes while also separating these components and preventing the elements in the electrode from diffusing into the TE materials and deteriorating the device performance[10,11]. The challenging aspect in contact design originates from the interface where the TE and contact materials connect with each other. The contact terminal is crucial to the band alignment at the interface, which is generally determined by the work function theory[12]. A buffer or transition phase can be created between the metal electrode and the TE material due to thermodynamically lower formation energy at a specific temperature or unsaturated bonding at the surfaces of the metal and the semiconductor. Such a new phase might cause ohmic contact failure or a break in the contact due to excessive thermal expansion, which also leads to the aging problem, or could act as a buffer zone that relieves the lattice mismatch and prevents elemental diffusion[13,14].

It has been demonstrated that most metallic materials can realize good ohmic contacts with TE materials. Materials incorporating Ni, Fe, Co, Ag, Mo, *etc.* have been tested as contacts for TE materials such as Bi_2Te_3, Mg_3Sb_2, Mg_2Si, PbTe, and half-Heusler compounds[10,15-18]. However, the underlying mechanism remains obscure, and there is no general rule to follow in contact design. As the main components of the most common contact materials, transition metals, such as Nb, Fe, Mn, Ta, Co, *etc.*, can effectively alter the charge-transport properties of the TE material[19]. This has recently been found for n-type Mg_3Sb_2[16,20], but it must be emphasized that contacts for Bi-rich n-type $Mg_{+\delta}Bi_{2-x}Sb_x$ have not yet been extensively explored. The phase diagrams or the formation energy values for Sb- and Bi-rich compounds in this system could be completely different when forming contacts with transition metals. Additionally, it has also come to our attention that bi- or tri-metal alloys have barely been considered as contact materials, although these can have mechanical and thermal advantages over a single metal.

Here, different metals (Ni and Fe) and metal alloys (NiFe, NiCr, NiFeCr, and stainless steel) were used to form contacts with an n-type $Mg_{3+\delta}Bi_{1.5}Sb_{0.5}$-based compound. All the contacts underwent aging for over 2100 h at 573 K, the designed maximum operating temperature. Contact reliability was then evaluated

under thermal cycling between 573 K and 433 K, followed by quenching in water. Contact resistivity and interfacial micro-morphology were carefully examined throughout the testing of each contact. NiFe exhibited the lowest contact resistivity over the entire aging, thermal cycling, and quenching process, and there were no observations of cracking or element diffusion across the contact interface. Additionally, a general rule is proposed for forming ohmic contacts for optimized TE materials. It was found that degenerated and heavily doped TE materials are ready to form low-resistivity ohmic contacts with metals or metal alloys and that thermal stability and thermal failure resistance are the major concerns for device development.

EXPERIMENTAL METHODS

Thermoelectric single legs - N-type $Mg_{3+\delta}Bi_{1.5}Sb_{0.5}$-based TE material powders were synthesized by high-energy ball-milling. For each element, Mg turnings and Sb and Bi shots were weighed according to the respective stoichiometric ratio, loaded into a stainless-steel jar, and milled for 2 h. Each single leg was subsequently made by one-step hot pressing. The contact material powders used as received here were stainless steel, NiCrFe, NiCr, NiFe, Fe, and Ni. An as-prepared $Mg_{3+\delta}Bi_{1.5}Sb_{0.5}$ powder and a contact powder were loaded into a graphite die following a contact material-TE material-contact material order. The entire sandwich structure was hot-pressed at 973 K for 10 min. The p-type $Fe/Bi_{0.4}Sb_{1.6}Te_3/Fe$ counterpart was produced by melting and hot-pressing. Stoichiometric amounts of Bi, Sb, and Te were weighed and loaded into a quartz tube that was sealed under high vacuum and placed inside a box furnace overnight at 1023 K. After melting, the ingot was milled into fine powder for the subsequent one-step hot-pressing. All the powder materials were handled in a glove box with an Ar atmosphere. X-ray diffraction spectra were obtained using a PANalytical multipurpose diffractometer with an X'celerator detector (PANalytical X'Pert Pro). The surface morphology and composition characterizations were investigated using a scanning electron microscope (LEO 1525). The electrical conductivity was evaluated by the four-point probe method using commercial ULVAC ZEM-3 equipment.

Thermal aging and thermal cycling testing - Each single Metal/TE material (M/TE) leg was sealed within a quartz tube with a high vacuum and placed inside a furnace with a constant temperature of 573 K for 2160 h. To determine aging-time dependence, contact resistivity was also evaluated several times during the aging process. The M/TE leg was loaded back into the sealed quartz tube after each measurement until the aging time reached 2160 h. Thermal cycling testing of each single M/TE leg was performed in a quartz tube with a high vacuum under controlled temperature cycles between 573 K and 433 K for ~100 cycles. The quartz tube containing the M/TE leg was then directly quenched from 573 K into cold water five times.

Contact resistance measurement - The contact resistance of each single M/TE leg was evaluated using homemade equipment. A constant current of 100 mA was provided by a power source connected to the contact ends of the single M/TE leg. The voltage changes between the contact material and the contact interface and between the interface and the TE material were collected at the surface by a scanning probe with a step length of 0.082~0.085 mm (the actual step length after the probe moving distance is normalized by the testing length of the M/TE leg).

Coefficient of thermal expansion (CTE) measurement - The CTE of each TE and contact material was evaluated over a temperature range between 300 K and 573 K. The measurements were carried out on a NETZSCH DIL 402C horizontal pushrod dilatometer with a He purge.

Preparation of the TE unicouple – The dimensions of each thermoelectric leg were calculated using the formula $\left\{\frac{A_1/l_1}{A_2/l_2}\right\} = \sqrt{\frac{\sigma_2\kappa_2}{\sigma_1\kappa_1}}$, where A, l, σ, and κ are the cross-section area, the length, the electrical conductivity, and

the thermal conductivity, respectively, of the thermoelectric leg. The total leg length is 4.516 mm, which includes the length of the thermoelectric materials (4 mm). The thermoelectric legs were joined with the electrodes by soldering using $In_{52}Sn_{48}$ (melting point ~391 K) and $Pb_{97}Sn_{1.5}Ag_{1.5}$ (melting point ~586 K) as the solder at the cold side and the hot side, respectively.

RESULTS AND DISCUSSION

Ohmic contact formation between a metal and a TE material

Metal/TE material (M/TE) contacts are critical to the performance of TE modules[21]. The ideal M/TE contact is expected to be ohmic, which means that the current flowing across the interface between the contact and the TE material (ICTE) should not encounter any barriers in either direction. When the intimate M/TE contact is established, the initial energy states of the metal and the TE material will be disrupted until a new equilibrium is reached around the interfacial region. The emerging band diagram is primarily determined by the work function of a metal (Φ_M) and of a semiconductor (Φ_S). Figure 1 illustrates the ideal energy band diagrams of a junction composed of a metal and an n-type semiconductor at equilibrium with the assumption of the absence of interfacial layer formation. In the case of $\Phi_M > \Phi_S$, shown in Figure 1A, electrons will flow downhill from the semiconductor to the metal until achieving equilibrium[22]. The transferred electrons create negative charges in the metal and positive charges in the semiconductor, resulting in a depletion region, and the aligned Fermi level gives rise to the Schottky barrier Φ_B, which leads to the rectifying effects of the junction as exhibited by the diodes. The ideal ohmic contact at the M/TE junction generally requires $\Phi_M < \Phi_S$, as shown in Figure 1B. The electrons are forced to flow toward the semiconductor from the metal until achieving equilibrium, leading to an electron-rich region at the ICTE and upward alignment of the Fermi level of the semiconductor. The ohmic contact leads to low resistance for the electron flow in both directions and is non-rectifying. It is worth mentioning that Φ_S is intimately dependent on doping concentration since there is a correlation between the work function and the Fermi level in semiconductors.

A requirement for achieving an ohmic contact or a non-rectifying barrier at the M/TE junction is that the work function of the n-type (p-type) semiconductor is larger (smaller) than that of the metal. However, the ICTE in a real situation is complicated and could exhibit strong dependence on interface properties, including morphology, preparation, gas on the surface, oxidation, *etc.*, which results in work functions that are significantly different after the contact is established in comparison with those obtained on the free surfaces[23]. Supplementary Table 1 shows the typical work functions of various metals, metal alloys, and TE materials. A comparison between these data and the reported experimental results suggests that the relative work function values could be a guide for forming a non-rectifying junction between specific materials, but they could not guarantee an ohmic contact at their ICTE[24].

TE materials are generally degenerate with a tuned narrow bandgap, which results in a relatively high carrier concentration ($>10^{19}$ cm^{-3})[25,26]. At an interface without the presence of diffusion, such high carrier concentration decreases the depletion region width, leading to a high probability of current flow through the barrier *via* tunneling rather than through thermionic emission. The tunneling model for an ohmic contact is proposed as $\rho_c \propto \exp(\alpha\Phi_B/\sqrt{n})$, where ρ_c is the contact resistivity, α is a material-related constant, and n is the carrier concentration[27]. This formula emphasizes the critical role of carrier concentration in realizing a low contact resistance. The occurrence of thermionic emission, on the other hand, requires electrons with sufficient energy to overcome the Schottky barrier, which in turn normally requires the presence of forward or reverse bias. There are two ways for the electrons to tunnel through the barrier junction, field emission (FE) and thermionic field emission (TFE), which dominate the electrons tunneling at low temperature and high temperature, respectively. The ratio E_{00}/K_BT generally is considered as the

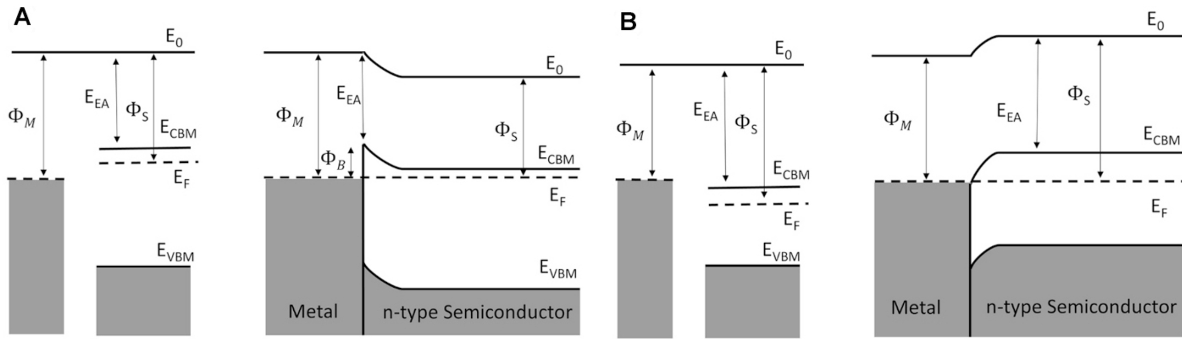

Figure 1. Band diagrams of a metal and an n-type semiconductor before (left) and after (right) forming the contact for the cases of (A) $\Phi M > \Phi S$; and (B) $\Phi M < \Phi S$.

standard gauge for evaluating the dominant current flow mechanism at the ICTE[28]. The characteristic energy E_{00} is defined as $E_{00} = \frac{q\hbar}{2}\sqrt{\frac{n}{m^{*}\varepsilon}}$, where q is the electronic charge; $\hbar$ is the reduced Planck constant; and n, m^*, and ε are the carrier concentration, effective mass, and dielectric constant of the semiconductor, respectively, and K_B and T are the Boltzmann constant and the temperature, respectively. When $E_{00}/K_BT \geq 0.2$, the TFE and FE processes dominate, indicating that the current flow is realized by tunneling through the depletion region. The characteristic parameters and calculated E_{00}/K_BT ratios of several TE materials are shown in Table 1. Clearly, the optimized TE materials shown can easily satisfy the $E_{00}/K_BT \geq 0.2$ condition for tunneling due to their relatively high carrier concentration. It has been demonstrated that low contact resistivity is readily achieved when forming contacts between these materials and Ni, Co, Fe, *etc*[34,35]. Additionally, most of the optimized TE materials are degenerate semiconductors, in which the Fermi level moves up into the conduction band (or down into the valence band), leading to the increased possibility of TFE or FE. The potential Schottky barrier Φ_B resulting from the aligned Fermi level can thus be substantially reduced, as shown in Figure 1, leading to an ohmic contact at the M/TE junction.

Ohmic contacts with low resistivity can thus be achieved by adhering to the rules discussed above. It is then quite important to maintain ICTE stability without expansion or cracking during device operation; otherwise, the contact resistance would increase considerably, leading to much lower efficiency or in the worst case, device failure.

Reliable contact formation with n-type $Mg_{3+\delta}Bi_{2-x}Sb_x$

It is reasonable that n-type $Mg_{3+\delta}Bi_{2-x}Sb_x$ compounds would form low-resistivity contacts with metal due to their high degeneracy and large carrier concentration. Here we examined the resistivity and reliability of the contacts formed between n-type $Mg_{3+\delta}Bi_{1.5}Sb_{0.5}$ and different metals and metal alloys. The detailed compositions of the metal alloys used (NiCr, NiFe, NiCrFe, and stainless steel) can be found in Supplementary Table 2. All contacts were produced by one-step hot-pressing to eliminate any avoidable contamination[36]. As shown in Supplementary Figure 1, the TE material was directly sandwiched between two layers of metal or metal alloy powders, which substantially diminished the surface states of the semiconductor and reduced the barrier at the ICTE. The contact resistance of each sample was evaluated using a homemade system with one probe scanning across the interface, and Figure 2 shows a schematic of the measurement setup and details of the method used to evaluate the measured contact resistivity data. As illustrated in Figure 2A, a constant current of 100 mA was supplied to the ends of a single TE leg composed of the TE material sandwiched by metallic contacts, and a scanning probe was adopted to collect the voltage variation across the contacts and the TE material. As shown in Figure 2B, the V-I curve exhibits differences

Table 1. Characteristic parameters and calculated E_{00}/K_BT ratios of various TE materials

	Effective mass (m_0)	Carrier concentration (10^{19} cm^{-3})	Dielectric constant	E_{00}/K_BT
PbTe	0.36	7.5	26	2.02[29]
SnSe	1	4	15	1.16[30]
$CoSb_3$	4.8	40	36	1.08[31]
NbCoSb	7.7	70	22	1.45[17]
Mg_2Si	2	20	20	1.60[32]
n-type Mg_3Sb_2	0.19	6.3	15	1.48[16]
$Bi_{0.5}Sb_{1.5}Te_3$	0.2	5	75	1.31[33]

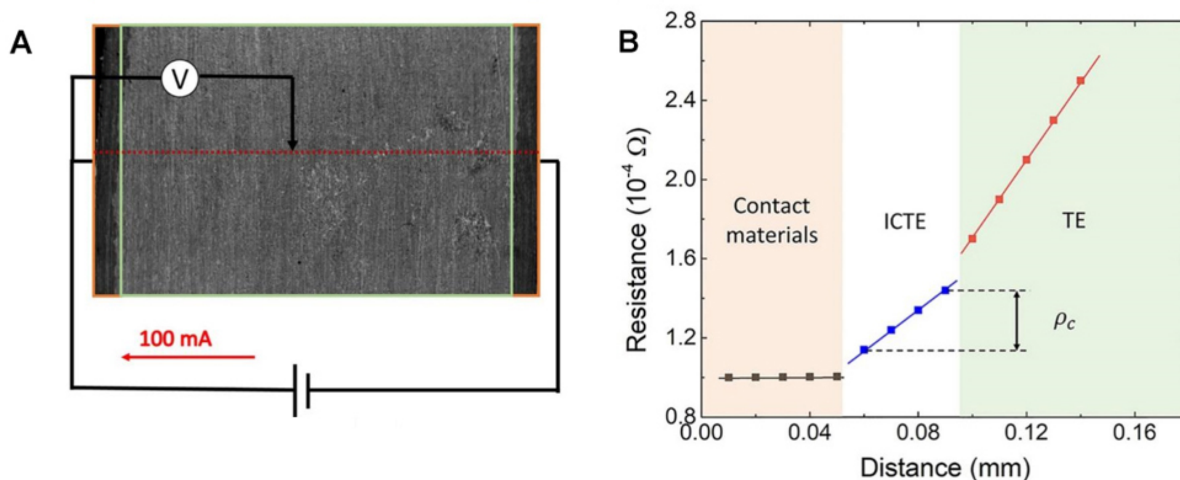

Figure 2. (A) Schematic of the contact resistivity measurement setup using homemade equipment. (B) Measured location-dependent contact resistance.

in its linear slope as the probe scans from the contact material to the ICTE and then to the TE material. The noticeable change in slope indicates the contact interface. The probe scans with a step length of around 82~85 μm, which is large enough to cover the interfacial thickness of the contact. The contact resistivity is expressed by $\rho_c = (\Delta V/I) \times A$, where ΔV, I and A are the step voltage change, current, and contact interfacial area, respectively.

All as-prepared M/TE contacts underwent aging for ~2100 h at 573 K, and the contact resistivity of each was measured as described above prior to and after aging. Comparisons of measured contact resistivity curves for each sample before and after aging are shown in Supplementary Figure 2. The simple linear slope for each sample suggests that ohmic contacts were successfully formed, which verifies the theoretical propositions discussed above. Additionally, the two curves shown in Figure 3A, the contact resistivity measured before and after the aging test of the sample composed of NiFe and n-type $Mg_{3+\delta}Bi_{1.5}Sb_{0.5}$, are reasonably comparable, which proves that long-term aging does not deteriorate the contact or the TE material. The post-aging slope shows a small change as an effect of the slightly decreased surface area resulting from the polishing and wiring of the surface for contact resistance measurements after aging (see Experimental Methods). Since the contact and TE materials are connected serially, the resistivity of each should be considered. The resistivity of the TE material, extracted from the slopes of the measured contact resistivity curves of different samples, still maintained the low values of around $1.48{\sim}1.57 \times 10^{-5}$ Ω m both prior to and after aging, as shown in Figure 3B, suggesting the good stability of n-type $Mg_{3+\delta}Bi_{1.5}Sb_{0.5}$ at 573 K. The resistivity of each contact material was extracted from its corresponding slope in the measured

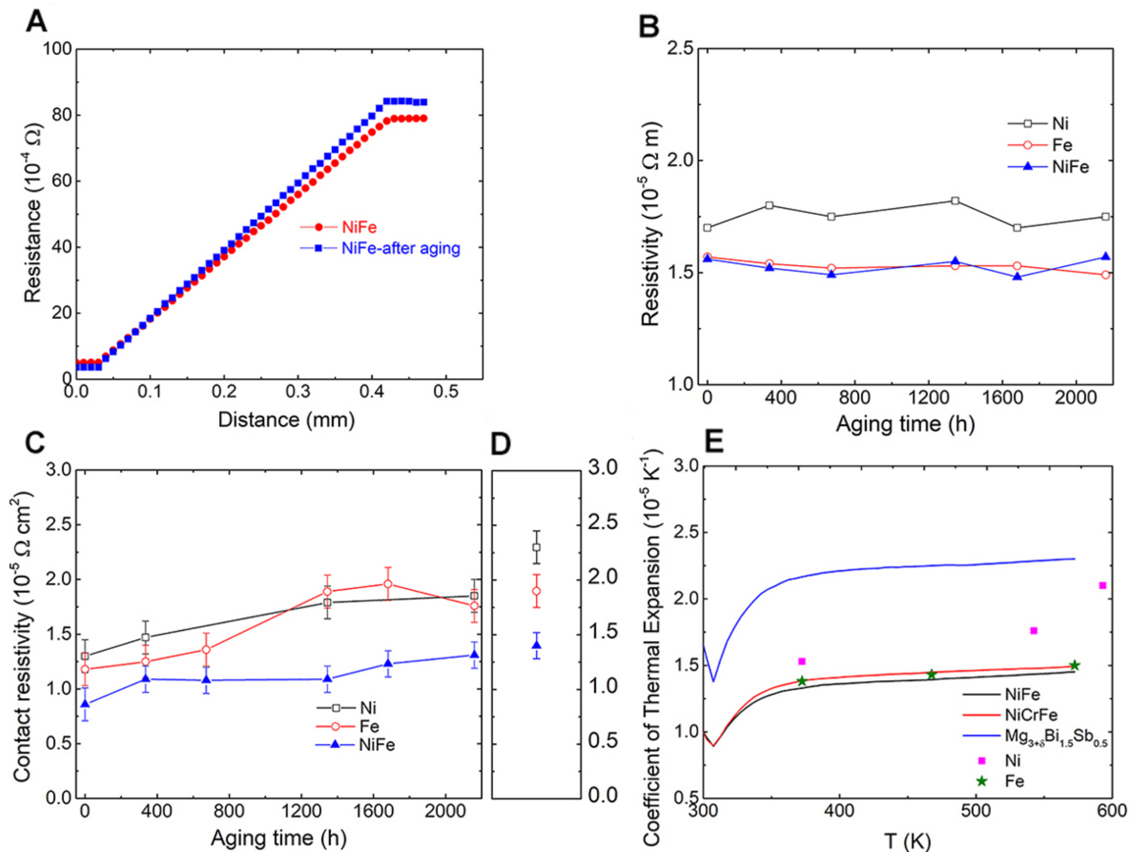

Figure 3. (A) Comparison of measured contact resistance before and after aging for ~2100 h at 573 K for the single TE leg composed of NiFe and n-type $Mg_{3+\delta}Bi_{1.5}Sb_{0.5}$. Aging-time dependence of (B) the resistivity of the TE material extracted from the slopes of the measured contact resistance curves [as shown, for example, in (A)] of different samples as specified and (C) the contact resistivity of single M/TE legs composed of n-type $Mg_{3+\delta}Bi_{1.5}Sb_{0.5}$ and different contact materials as specified. (D) contact resistivity of single TE legs composed of n-type $Mg_{3+\delta}Bi_{1.5}Sb_{0.5}$ and different contact materials as specified after temperature cycling and quenching. (E) temperature-dependent CTE values of NiFe, NiCrFe, and $Mg_{3+\delta}Bi_{1.5}Sb_{0.5}$ in comparison with those of Ni and Fe.

contact resistivity curves [Supplementary Figure 2] and is shown in Supplementary Figure 3. Additionally, the contact materials were independently pressed following the procedure for preparing the single M/TE legs, and their resistivity values were also verified using a commercial ULVAC ZEM-3. It was determined that NiFe exhibits competitively low resistivity in comparison with the other contact materials studied.

The aging-time dependences of the contact resistivity of M/TE contacts using NiFe, Ni, and Fe are shown in Figure 3C, along with NiCr, NiFeCr and stainless steel shown in Supplementary Figure 4A Among these samples, that prepared with the NiFe alloy exhibits the lowest contact resistivity, and its contact resistivity has the slowest rate of increase over the entire aging process. As shown in Supplementary Figure 4, the NiFe/TE contact also outperforms those prepared with NiCr, NiCrFe, and stainless steel. After aging for over 2100 h, NiFe/TE exhibits the smallest contact resistivity, ~1.30×10^{-5} Ω cm^2, which is nearly comparable with that of Mg_3Sb_2/stainless steel after aging for 400 h (1.16×10^{-5} Ω cm^2) and lower than that of NbFeSb/Mo after aging for 768 h (1.84×10^{-5} Ω cm^2)[16,37].

Following aging testing, each of the single TE leg samples underwent temperature cycling between 433 K and 573 K and subsequent quenching. As shown in Figure 3D and Supplementary Figure 4B, after undergoing such harsh tests, the contact resistivity of each sample was found to be higher than its post-

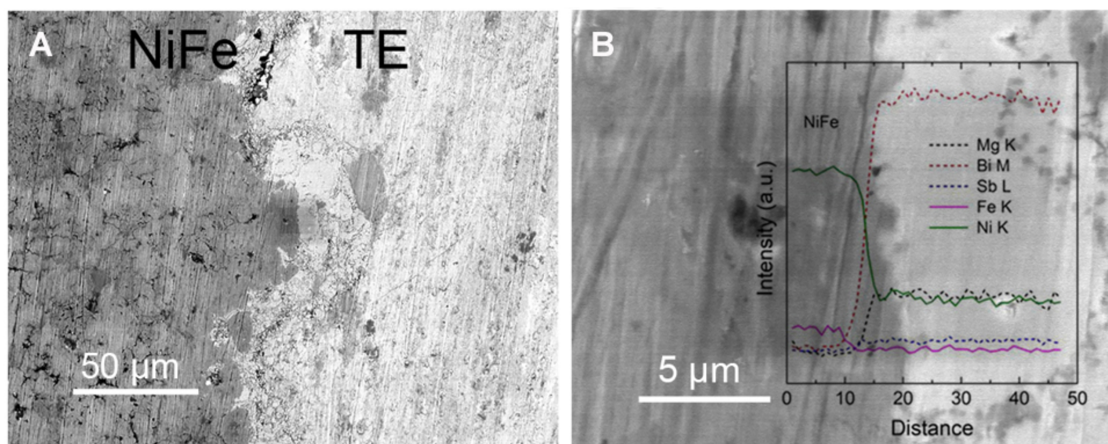

Figure 4. Microstructural morphology of the contact interface in the single TE leg sample composed of NiFe and $Mg_{3+\delta}Bi_{1.5}Sb_{0.5}$ after aging and thermal cycling and quenching. Inset in (B): EDS line scan across the contact interface in the same sample.

aging value and that of NiFe/TE remained the lowest after rising only slightly. Given the actual operating parameters of a TE power generator, the two ends of the TE leg need to withstand safely a temperature difference of around 100~200 K. Excellent resistance to thermal stress is crucial for the contacts. The temperature-dependent coefficient of thermal expansion (CTE) values of NiFe, NiCrFe, and $Mg_{3+\delta}Bi_{1.5}Sb_{0.5}$, along with those of Ni and Fe, are displayed in Figure 3E, which shows that the CTE matching between the TE and contact materials is acceptable.

The ICTE microstructures in the single M/TE legs prior to and after aging and thermal cycling evaluation were examined and are shown in Supplementary Figure 5 and Supplementary Figure 6, respectively. It can be observed in Supplementary Figure 5 that the contact bonding between each metal or metal alloy and the TE material was well established by one-step hot pressing. All the interfaces are clearly visible, and there are no noticeable cracks at the ICTE. There are tiny dents and pores along the ICTE of NiCrFe/TE and stainless steel/TE. It is difficult to state conclusively whether these dents and pores result from the hot-pressing process, interfacial reaction, or polishing, but the contact resistivity measurements show that an ohmic contact was formed in each case. Figure 4A shows the microscopic morphology of the contact interface of the NiFe/$Mg_{3+\delta}Bi_{1.5}Sb_{0.5}$. It can be observed that the interface is well-defined and that it remained clean and intact after aging and thermal cycling testing. However, tiny cracks are present in the area around the interface in the samples prepared using Ni, NiCr, NiCrFe, and stainless steel, as shown in Supplementary Figure 6, which is directly reflected by their high contact resistivity values as shown in Supplementary Figure 3. An energy-dispersive X-ray spectroscopy (EDS) line scan across the ICTE in the NiFe sample [Figure 4B] shows that the composition changes sharply over a short range, where the concentrations of Ni, Bi, and Mg vary in a linear transition. It should also be noted that no cracks are found at the interface in the sample prepared using Fe. Revisiting the compositions of the metal alloys used here [Supplementary Table 1], it is speculated that the 20% Fe content in the NiFe alloy might be the reason that its corresponding ICTE is protected from cracking. On the other hand, among the CTE values of Ni, Fe, NiFe, and NiCrFe shown in Figure 3E, that of Ni clearly increases the most over the temperature range examined.

Interfacial or transition phase evolution at an ICTE is closely correlated with the length of service life for the TE module. Due to the bonding process at the interface, diffusion, reaction, or both are inevitable phenomena at the ICTE and could possibly accelerate the progress of device failure. It is thus imperative to

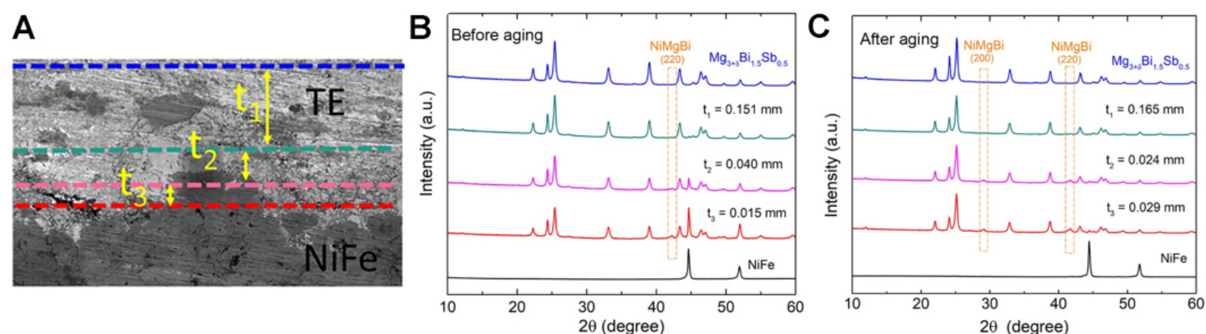

Figure 5. XRD patterns obtained at different heights across the ICTE in the NiFe/$Mg_{3+\delta}Bi_{1.5}Sb_{0.5}$ sample. (A) Schematic illustration of the data collection showing that, after the initial XRD pattern was obtained, further data were collected after each polishing to remove layers with thicknesses t_1, t_2, and t_3, as specified in (B and C). XRD patterns obtained across the ICTE (B) prior to and (C) after aging. The dashed blue, dark cyan, magenta, and red lines in (A) indicate the XRD collecting surfaces corresponding to the XRD patterns in (B and C).

determine the interfacial situation following aging. For n-type Mg_3Bi_2-based compounds, the interlayer potentially could act as a diffusion channel due to the layer structure. It was demonstrated that diffusion occurs at the ICTE for contacts incorporating Bi_2Te_3[38]. X-ray diffraction (XRD) patterns were obtained across the ICTE in NiFe/$Mg_{3+\delta}Bi_{1.5}Sb_{0.5}$ prior to and after aging and thermal cycling evaluation to verify whether diffusion or interfacial phases had emerged. XRD patterns in Figure 5 obtained at different sample heights confirm that all the diffraction peaks on the TE material side away from the ICTE align well with pure $Mg_{3+\delta}Bi_{1.5}Sb_{0.5}$, indicating that there was no elemental diffusion from the NiFe contact material across the ICTE. The same is true for the NiFe side. It is noticed that the central peak of NiFe in Figure 5C is weak because the polishing depth is not high enough to reach the rich side of NiFe contact. A tiny peak located at 41.67° in the pre-aging XRD patterns was identified as the (220) plane of NiMgBi (PDF#06-0231). NiMgBi is a metal with a cubic crystal structure (data obtained from the Materials Project) and shows no detrimental influence on the electron transport across the ICTE. The XRD patterns obtained after aging and thermal cycling testing clearly show the phase evolution crossing the ICTE. There is an additional emerging peak at 29.06° corresponding to the (200) plane of NiMgBi, which is in accordance with the observation from the EDS line scan in the inset to Figure 4B that there is a narrow space for the Ni, Mg, and Bi to transition across the ICTE. The formation of NiMgBi at the interface could effectively prevent elemental diffusion without undermining the electron transfer, which is most likely the reason that no peaks shift in the XRD patterns.

Energy conversion efficiency of a thermoelectric power generator (TEG)

There is strong competition between thermoelectric power generation/refrigeration and Joule heating, which positively correlates with the input current applied on the load. High contact resistance could thus severely compromise the performance of a thermoelectric device due to the accompanying Joule heating. To verify the performance improvement of a TEG that could result from low contact resistance, a unicouple was assembled with NiFe/$Mg_{3+\delta}Bi_{1.5}Sb_{0.5}$ as the n-type leg and a p-type counterpart made *via* one-step pressing using $Bi_{0.4}Sb_{1.6}Te_3$ as the TE material and Fe as the contact material, and its energy conversion efficiency was measured using a homemade setup as shown in Figure 6A[5,21]. The thermoelectric transport properties of the TE materials were properly optimized toward room-temperature operation as shown in Supplementary Figure 7. The contact resistance measurement in Supplementary Figure 8 confirms the low contact resistance of the n-type leg achieved here. We would like to emphasize device performance at small temperature differences near room temperature where the n- and p-type counterparts exhibit peak performance. Here the cold-side temperature was maintained around room temperature. The open circuit voltage (V_{oc}), output power and heat flowing through the heat sink (Q_{in}) of the unicouple at different hot-

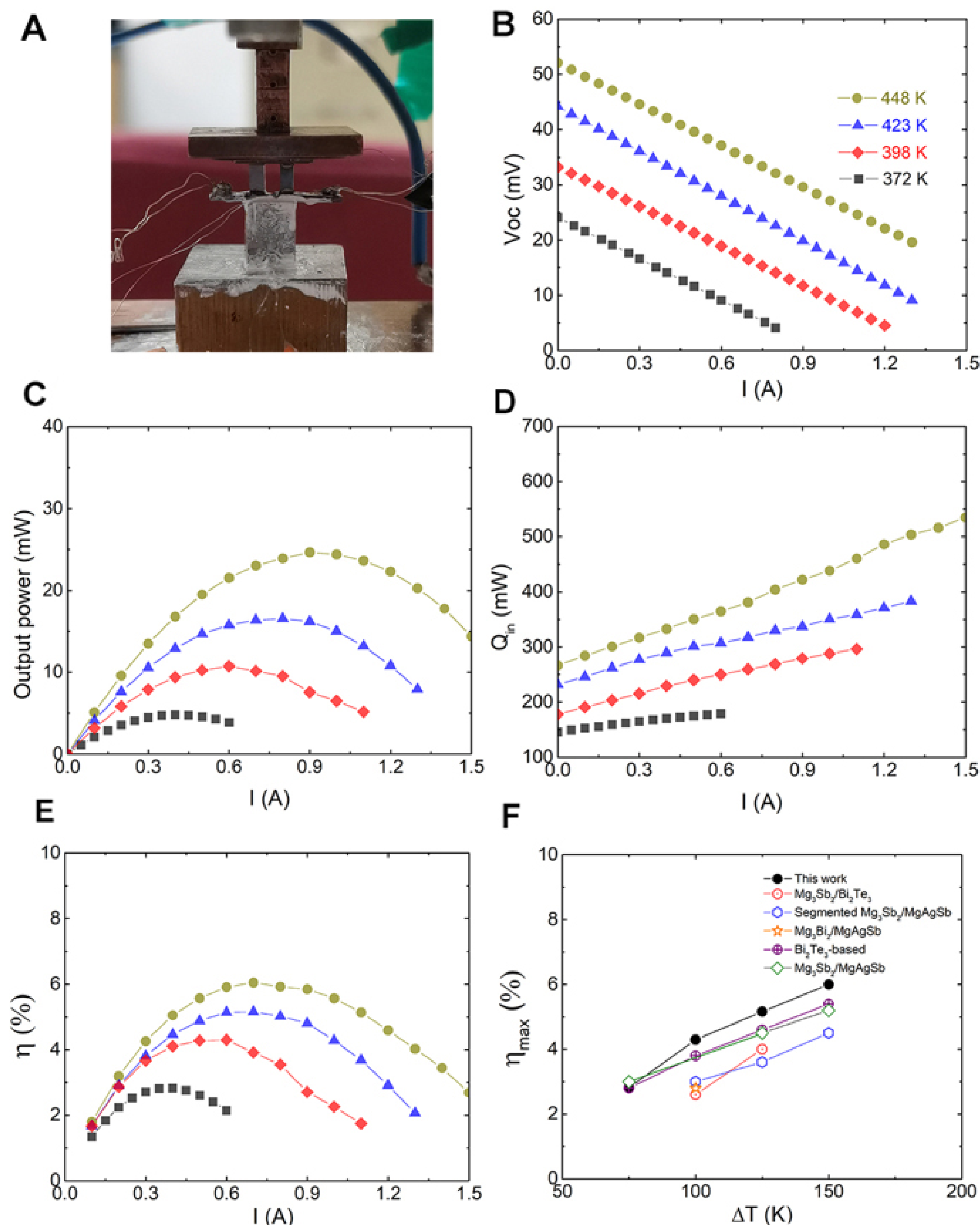

Figure 6. Conversion efficiency measurement of a $Mg_{3+\delta}Bi_{1.5}Sb_{0.5}/Bi_{0.4}Sb_{1.6}Te_3$ unicouple with the cold-side temperature maintained at room temperature. (A) Unicouple measurement setup. Input current relationship with (B) open circuit voltage, (C) output power, (D) heat flow out of the cold side, and (E) conversion efficiency at different hot-side temperatures. (F) comparison of conversion efficiency between this work and recently reported devices operating at near room temperatures (Mg_3Sb_2/Bi_2Te_3[6], Bi_2Te_3-based device[9], segmented $Mg_3Sb_2/MgAgSb$[38], $Mg_3Bi_2/MgAgSb$[40], and $Mg_3Sb_2/MgAgSb$[43]).

side temperature as variation of the current were recorded in Figure 6B-D, respectively. Benefiting from the low contact resistance and the properly optimized n- and p-type materials, the $Mg_{3+\delta}Bi_{1.5}Sb_{0.5}/Bi_{0.4}Sb_{1.6}Te_3$ unicouple achieved conversion efficiency of ~4% at a temperature difference of 100 K [Figure 6E], which is better than the cutting-edge results reported recently [Figure 6F][9,39-41]. The highest efficiency obtained was

~6% at a temperature difference of 150 K and a hot-side temperature of 448 K. With such a decent efficiency, this unicouple already outperforms an intermediate TEG with a temperature difference of over 400 K[5,42,43].

CONCLUSION

The high degeneracy and large carrier concentration of optimized TE materials indicate that they are ready to form ohmic contacts with metals and metal alloys, which was successfully verified by the low-resistance contact achieved in NiFe/$Mg_{3+\delta}Bi_{1.5}Sb_{0.5}$ here. After long-term aging followed by temperature cycling and quenching, thermoelectric single-leg NiFe/$Mg_{3+\delta}Bi_{1.5}Sb_{0.5}$ showed the lowest contact resistivity among those studied and no cracks were observed across its contact interface. It was found that metallic NiMgBi formed as a buffer phase at the interface of NiFe and $Mg_{3+\delta}Bi_{1.5}Sb_{0.5}$, which could effectively prevent elemental diffusion and shows no harm to the electron transport. Most importantly, the resistivity of the NiFe alloy itself is quite competitively low. To demonstrate that NiFe can be a reliable contact for the n-type $Mg_{3+\delta}Bi_{2-x}Sb_x$, a unicouple composed of n-type NiFe/$Mg_{3+\delta}Bi_{1.5}Sb_{0.5}$ and p-type Fe/$Bi_{0.4}Sb_{1.6}Te_3$ was assembled. Conversion efficiency values of ~4% and ~6% were achieved with temperature differences of 100 K and 150 K, respectively, and with the cold-side temperature maintained at room temperature, indicating that this unicouple outperforms most cutting-edge low- and intermediate-temperature thermoelectric power generators.

DECLARATIONS

Authors' contributions

Conceived and designed the work: Song S, Ren Z
Conducted the measurement and data recording: Song S, Liang Z, Xu C
Made the contacts and unicouple: Song S, Wang Y
Analyzed the data: Song S, Liang Z, Xu C, Shi X, Ren W
Was involved in the manuscript writing and revision: Song S, Liang Z, Xu C, Wang Y, Shi X, Ren W, Ren Z

Availability of data and materials

Not applicable.

Financial support and sponsorship

Ren Z acknowledges support from Alexander von Humboldt foundation and Professor Kornelius Nielsch at IFW-Dresden, Germany.

Conflicts of interest

All authors declared that there are no conflicts of interest.

Ethical approval and consent to participate

Not applicable.

Consent for publication

Not applicable.

Copyright

© The Author(s) 2022.

REFERENCES

1. Tamaki H, Sato HK, Kanno T. Isotropic conduction network and defect chemistry in $Mg_{3+\delta}Sb_2$-based layered zintl compounds with high thermoelectric performance. *Adv Mater* 2016;28:10182-7. DOI PubMed
2. Han Z, Gui Z, Zhu YB, et al. The electronic transport channel protection and tuning in real space to boost the thermoelectric performance of $Mg_{3+\delta}Sb_{2-y}Bi_y$ near room temperature. *Research (Wash D C)* 2020;2020:1672051. DOI
3. Mao J, Zhu H, Ding Z, et al. High thermoelectric cooling performance of n-type Mg_3Bi_2-based materials. *Science* 2019;365:495-8. DOI PubMed
4. Chen L, Zhang Q, Guo Z, et al. Expand band gap and suppress bipolar excitation to optimize thermoelectric performance of Bi0.35Sb1.65Te3 sintered materials. *Mater Today Phys* 2021;21:100544. DOI
5. Liang Z, Xu C, Shang H, et al. High thermoelectric energy conversion efficiency of a unicouple of n-type Mg3Bi2 and p-type Bi2Te3. *Mater Today Phys* 2021;19:100413. DOI
6. Xu C, Liang Z, Shang H, et al. Scalable synthesis of n-type Mg3Sb2-xBix for thermoelectric applications. *Mater Today Phys* 2021;17:100336. DOI
7. Shang H, Liang Z, Xu C, et al. N-type Mg3Sb2-Bi with improved thermal stability for thermoelectric power generation. *Acta Materialia* 2020;201:572-9. DOI
8. Zheng G, Su X, Xie H, et al. High thermoelectric performance of p-BiSbTe compounds prepared by ultra-fast thermally induced reaction. *Energy Environ Sci* 2017;10:2638-52. DOI
9. Zhu B, Liu X, Wang Q, et al. Realizing record high performance in n-type Bi_2Te_3-based thermoelectric materials. *Energy Environ Sci* 2020;13:2106-14. DOI
10. Sakamoto T, Taguchi Y, Kutsuwa T, Ichimi K, Kasatani S, Inada M. Investigation of barrier-layer materials for Mg2Si/Ni interfaces. *J Electron Mater* 2016;45:1321-7. DOI
11. Ofuonye B, Lee J, Yan M, Sun C, Zuo J, Adesida I. Electrical and microstructural properties of thermally annealed Ni/Au and Ni/Pt/Au schottky contacts on AlGaN/GaN heterostructures. *Semicond Sci Technol* 2014;29:095005. DOI
12. Xiong K, Wang W, Alshareef HN, et al. Electronic structures and stability of Ni/Bi_2Te_3 and Co/Bi_2Te_3 interfaces. *J Phys D Appl Phys* 2010;43:115303. DOI
13. Monch W. On the physics of metal-semiconductor interfaces. *Rep Prog Phys* 1990;53:221-78. DOI
14. Huang D, Shang H, Li T, et al. Superconducting joining of YBCO coated conductors without a large critical current loss. *Mater Today Phys* 2021;21:100567. DOI
15. Hu X, Jood P, Ohta M, et al. Power generation from nanostructured PbTe-based thermoelectrics: comprehensive development from materials to modules. *Energy Environ Sci* 2016;9:517-29. DOI
16. Wang X, Xue W, Zhang Z, et al. Stabilizing the optimal carrier concentration in Al/Sb-Codoped GeTe for high thermoelectric performance. *ACS Appl Mater Interfaces* 2021;13:45717-25. DOI PubMed
17. Spataru CD, He Y, Léonard F. Atomistic study of an ideal metal/thermoelectric contact: the full-Heusler/half-Heusler interface. *APL Mater* 2019;7:013202. DOI
18. Liu W, Bai S. Thermoelectric interface materials: a perspective to the challenge of thermoelectric power generation module. *J Mater* 2019;5:321-36. DOI
19. Shuai J, Mao J, Song S, et al. Tuning the carrier scattering mechanism to effectively improve the thermoelectric properties. *Energy Environ Sci* 2017;10:799-807. DOI
20. Song S, Mao J, Bordelon M, et al. Joint effect of magnesium and yttrium on enhancing thermoelectric properties of n-type Zintl Mg3+Y0.02Sb1.5Bi0.5. *Mater Today Phys* 2019;8:25-33. DOI
21. Zhu Q, Song S, Zhu H, Ren Z. Realizing high conversion efficiency of Mg3Sb2-based thermoelectric materials. *J Power Sources* 2019;414:393-400. DOI
22. Yu A. Electron tunneling and contact resistance of metal-silicon contact barriers. *Solid-State Elect* 1970;13:239-47. DOI
23. Shao G. Work function and electron affinity of semiconductors: doping effect and complication due to fermi level pinning. *Energy Environ Mater* 2021;4:273-6. DOI
24. Zhang B, Zheng T, Wang Q, et al. Contact resistance and stability study for Au, Ti, Hf and Ni contacts on thin-film Mg2Si. *J Alloys Comp* 2017;699:1134-9. DOI
25. Xin J, Li G, Auffermann G, et al. Growth and transport properties of Mg3X2 (X = Sb, Bi) single crystals. *Mater Today Phys* 2018;7:61-8. DOI
26. Song S, Xu C, Liang Z, Ren Z. The challenge of tuning the ratio of lattice/total thermal conductivity toward conversion efficiency vs power density. *Appl Phys Lett* 2021;119:180501. DOI
27. Waldrop JR, Grant RW. Correlation of interface composition and barrier height for model AuGeNi contacts to GaAs Appl Phys Lett 1987. pp. 250-2.. DOI
28. Bartolomeo A. Graphene schottky diodes: an experimental review of the rectifying graphene/semiconductor heterojunction. *Phys Rep* 2016;606:1-58. DOI
29. Qin C, Cheng L, Xiao Y, et al. Substitutions and dislocations enabled extraordinary n-type thermoelectric PbTe. *Mater Today Phys* 2021;17:100355. DOI
30. Li S, Lou X, Zou B, et al. Introducing PbSe quantum dots and manipulating lattice strain contributing to high thermoelectric performance in polycrystalline SnSe. *Mater Today Phys* 2021;21:100542. DOI

31. Lei Y, Gao W, Zheng R, et al. Ultrafast synthesis of Te-Doped $CoSb_3$ with excellent thermoelectric properties. *ACS Appl Energy Mater* 2019;2:4477-85. DOI
32. Liu W, Tan X, Yin K, et al. Convergence of conduction bands as a means of enhancing thermoelectric performance of n-type Mg2Si(1-x)Sn(x) solid solutions. *Phys Rev Lett* 2012;108:166601. DOI PubMed
33. Yang KJ, Kim S, Kim SY, et al. Flexible $Cu_2ZnSn(S,Se)_4$ solar cells with over 10% efficiency and methods of enlarging the cell area. *Nat Commun* 2019;10:2959. DOI PubMed PMC
34. Kauzlarich SM, Brown SR, Snyder GJ. Zintl phases for thermoelectric devices. *Dalton Trans* 2007;12:2099-107. DOI PubMed
35. Hao F, Qiu P, Tang Y, et al. High efficiency Bi_2Te_3-based materials and devices for thermoelectric power generation between 100 and 300 °C. *Energy Environ Sci* 2016;9:3120-7. DOI
36. Himpsel FJ, Hollinger G, Pollak RA. Determination of the Fermi-level pinning position at Si(111) surfaces. *Phys Rev B* 1983;28:7014-8. DOI
37. Shen J, Wang Z, Chu J, et al. Low contact resistivity and interfacial behavior of p-Type NbFeSb/Mo thermoelectric junction. *ACS Appl Mater Interfaces* 2019;11:14182-90. DOI PubMed
38. Jia N, Cao J, Tan XY, et al. Thermoelectric materials and transport physics. *Mater Today Phys* 2021;21:100519. DOI
39. Ying P, He R, Mao J, et al. Towards tellurium-free thermoelectric modules for power generation from low-grade heat. *Nat Commun* 2021;12:1121. DOI PubMed PMC
40. Liu Z, Sato N, Gao W, et al. Demonstration of ultrahigh thermoelectric efficiency of ~7.3% in Mg3Sb2/MgAgSb module for low-temperature energy harvesting. *Joule* 2021;5:1196-208. DOI
41. Liu Z, Gao W, Oshima H, Nagase K, Lee CH, Mori T. Maximizing the performance of n-type Mg_3Bi_2 based materials for room-temperature power generation and thermoelectric cooling. *Nat Commun* 2022;13:1120. DOI PubMed PMC
42. Bu Z, Zhang X, Hu Y, et al. A record thermoelectric efficiency in tellurium-free modules for low-grade waste heat recovery. *Nat Commun* 2022;13:237. DOI PubMed PMC
43. Ying P, Wilkens L, Reith H, et al. A robust thermoelectric module based on MgAgSb/Mg_3 $(Sb,Bi)_2$ with a conversion efficiency of 8.5% and a maximum cooling of 72 K. *Energy Environ Sci* 2022;15:2557-66. DOI